Molecular-Level Functional Magnetic Resonance Imaging of Dopaminergic Signaling

Taekwan Lee,[1] Lili X. Cai,[1] Victor S. Lelyveld,[1] Aviad Hai,[1] Alan Jasanoff[1,2,3]*

We demonstrate a technique for mapping brain activity that combines molecular specificity and spatial coverage using a neurotransmitter sensor detectable by magnetic resonance imaging (MRI). This molecular functional MRI (fMRI) method yielded time-resolved volumetric measurements of dopamine release evoked by reward-related lateral hypothalamic brain stimulation of rats injected with the neurotransmitter sensor. Peak dopamine concentrations and release rates were observed in the anterior nucleus accumbens core. Substantial dopamine transients were also present in more caudal areas. Dopamine-release amplitudes correlated with the rostrocaudal stimulation coordinate, suggesting participation of hypothalamic circuitry in modulating dopamine responses. This work provides a foundation for development and application of quantitative molecular fMRI techniques targeted toward numerous components of neural physiology.

Despite development of magnetic resonance imaging (MRI) contrast agents sensitive to molecular aspects of brain function (*1*), neural activity mapping using such probes has not previously been demonstrated. Molecular imaging using contrast agents could provide a powerful method for determining topography and dynamics of neural activity components over brain volumes inaccessible to conventional electrophysiology or optical imaging. MRI-based molecular mapping would also substantially exceed the spatiotemporal resolution of positron emission tomography.

A prime target for molecular functional MRI (fMRI) is the ventral striatum, a brain region that integrates multiple neurochemically and anatomically defined neural populations involved in motivated behavior. Particular interest focuses on dopaminergic striatal afferents that project from the midbrain (*2*). These cells are phasically activated by rewards and reward-predictive cues (*3*) and are targets of drugs that boost striatal dopamine concentrations (*4*). Although neuroarchitecture of dopaminergic systems (*5*) and some regional differences in dopamine release have been studied (*6*), spatial aspects of signaling are generally less well understood. This complicates characterization of relationships among dopamine neuron firing, dopamine release, and broader neural activity.

Neurotransmitter-sensitive MRI contrast agents that we recently developed (*7*) could be used for mapping dopamine signaling in living brains. These probes are engineered forms of BM3h, a paramagnetic heme protein that alters T_1-weighted MRI signals. BM3h-based contrast agents can be injected intracranially to fill volumes of several cubic millimeters, comparable in size to the entire ventral striatum. A BM3h sensor variant called BM3h-9D7 displays optimal specificity for dopamine (dissociation constant K_d = 1.3 μM) versus norepinephrine (K_d = 37 μM) and serotonin (K_d = 70 μM) (*8*). Longitudinal relaxivity (r_1) of BM3h-9D7 at 37°C was measured to be 0.83 ± 0.01 and 0.10 ± 0.00 mM^{-1} s^{-1} in the absence and presence of saturating dopamine, respectively (fig. S1). These r_1 values imply that T_1-weighted MRI signal decreases are expected when dopamine is released in the presence of sensor.

We applied BM3h-9D7 in conjunction with electrical stimulation of the medial forebrain bundle (MFB) in lateral hypothalamus (LH); MFB microstimulation engages mesolimbic dopamine fibers (*9*) and is the basis for common addiction models. Rats were implanted with striatal injection cannulae and MFB-targeted electrodes (Fig. 1A) and assessed for operant performance in a self-stimulation task. Animals that learned the behavior were anesthetized and inserted into a 9.4-T MRI scanner. L-3,4-Dihydroxyphenylalanine (L-DOPA, 160 mg per kilogram of body weight) was injected to prevent dopamine depletion, and a relatively low dose of dopamine reuptake blocker, GBR-12909 (8 mg/kg), was administered to enhance synaptic overflow (*10*); these treatments promoted robust repeated measurements, but were not required for MRI signal changes (fig. S2). BM3h-9D7 (500 μM) was infused at 0.1 μl/min (Fig. 1B). After a 42-min preinjection period, periodic MFB stimuli were delivered in blocks of 16 s, separated by 5-min rest periods. T_1-weighted images were collected every 8 s throughout.

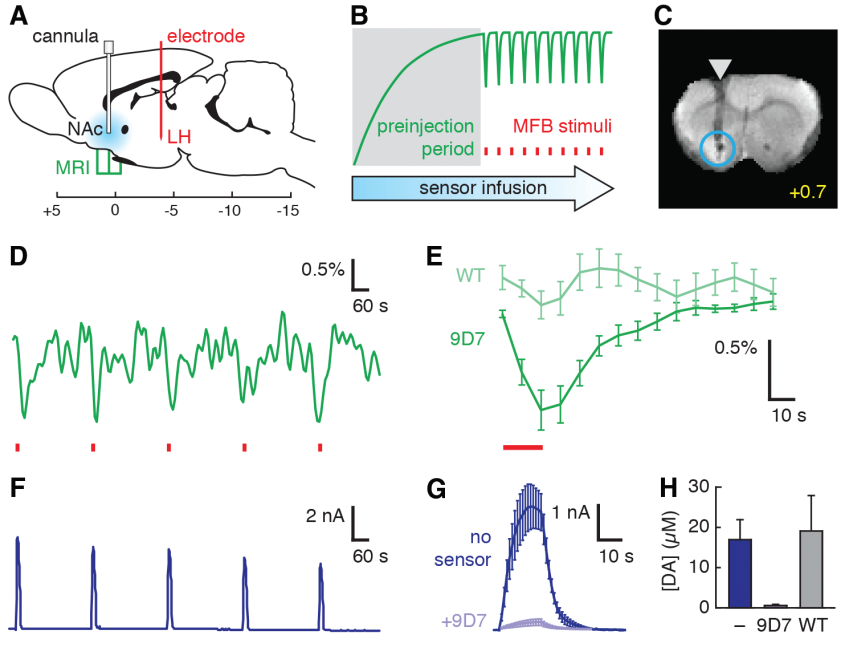

Fig. 1. Molecular fMRI detects dopamine signaling in ventral striatum. (**A**) Stimulation electrodes (red) were implanted in LH. Cannulae in NAc allowed dopamine sensor infusion (blue), and MRI data were acquired from surrounding slices. Scale shows coordinates relative to bregma. (**B**) Experimental design: Sensor preinjection (gray shading) is followed by functional imaging with MFB stimulation (red ticks). Green line represents expected MRI signal changes due to injection and stimulus-induced dopamine release. (**C**) Coronal slice (bregma + 0.7 mm) from a single rat brain after preinjection with BM3h-9D7. Arrowhead denotes cannula and circle defines an ROI. (**D**) ROI-averaged MRI signal over five stimuli (red ticks) in one animal, after preinjection of BM3h-9D7. (**E**) Average peristimulus IRF calculated within the ROI from animals injected with BM3h-9D7 (dark green, n = 7) or control BM3h-WT (light green, n = 7). Stimulation period indicated by red line. (**F**) Amperometric measurement of NAc dopamine release evoked by MFB stimuli (red ticks). (**G**) Average (n = 4) amperometry transients before (dark blue) or after (light blue) infusion of BM3h-9D7 (red line indicates stimulation period). (**H**) Calibrated dopamine amplitudes measured without sensor infusion (dark blue, n = 7), after infusion of BM3h-9D7 (light blue, n = 4), or after infusion of BM3h-WT (gray, n = 3). Error bars denote SEMs.

[1]Department of Biological Engineering, Massachusetts Institute of Technology (MIT), Cambridge, MA 02139, USA. [2]Department of Brain and Cognitive Sciences, MIT, Cambridge, MA 02139, USA. [3]Department of Nuclear Science and Engineering, MIT, 77 Massachusetts Avenue, Room 16-561, Cambridge, MA 02139, USA.

*Corresponding author. E-mail: jasanoff@mit.edu

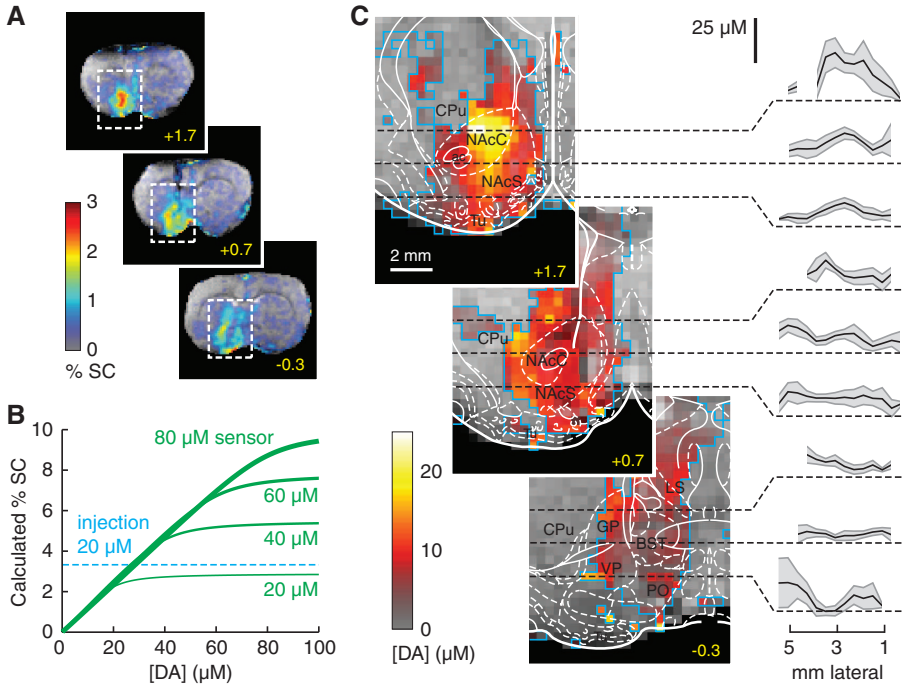

Fig. 2. Quantitative functional imaging of dopamine concentrations. (**A**) Raw maps of signal change averaged over seven animals injected with BM3h-9D7. Distribution of percent signal change (% SC) over three coronal sections; rostrocaudal coordinates in yellow. (**B**) Calculated % SC as a function of released dopamine concentration ([DA]) for four sensor concentrations, showing linearity of % SC versus [DA], except for saturation effects. In areas that received substantial contrast agent infusion, a ratio of 8 μM dopamine per % SC can be used to estimate dopamine concentrations. (**C**) Quantitative mapping of average peak dopamine concentrations over regions outlined in (A). Blue outlines indicate voxels included in the analysis, each incorporating data from two to seven animals (compare fig. S3). Rat brain atlas (*20*) is overlaid with labels in black; regions defined in text, plus anterior commissure (ac), bed nucleus of the stria terminalis (BST), globus pallidus (GP), lateral septum (LS), olfactory tubercle (Tu), and ventral pallidum (VP). Plots show means (black lines) and SEMs (shading) of dopamine concentrations along dashed lines in respective images.

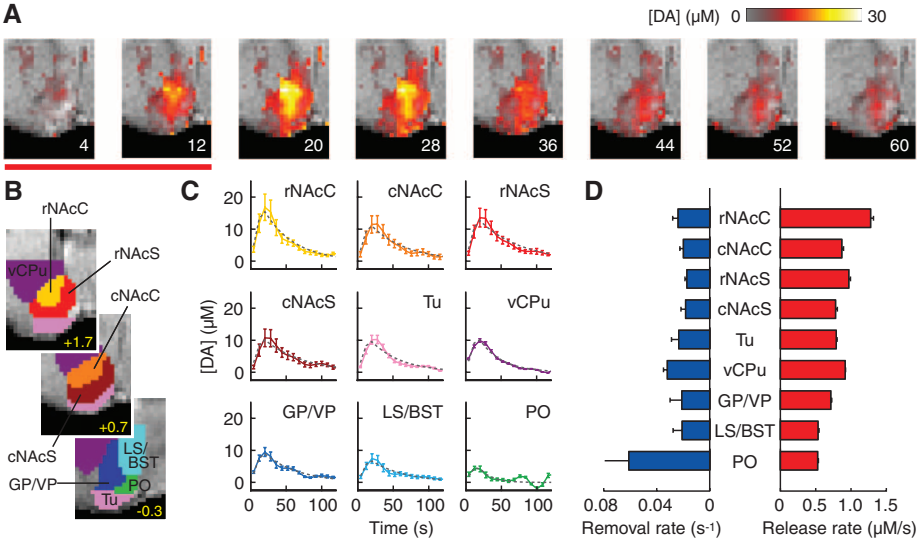

Fig. 3. Dynamics of dopamine-dependent MRI responses to MFB stimulation. (**A**) Image frames from the first eight time points of the IRF. Color bar indicates dopamine concentrations during and after an MFB stimulus (red line). (**B**) ROIs defined by brain atlas alignment to MRI data. (**C**) IRFs calculated for each ROI. Data points indicate mean [DA] at each time. Gray dashed lines show best-fit simulated time courses using a single compartment model. (**D**) Dopamine release (red) and removal (blue) rates estimated from model fitting. SEMs computed by jackknife resampling over seven animals.

MRI signal was examined in a region of interest (ROI) around the cannula tip (Fig. 1C). Transient signal decreases were observed with each stimulus (Fig. 1D). A peristimulus impulse response function (IRF) was calculated from each data set and averaged over seven animals (Fig. 1E). An average maximum signal decrease of 1.1 ± 0.2% was observed, peaking around the stimulus offset time; this change was statistically significant (Student's *t* test, $P = 0.0008$). Control experiments were performed with BM3h-WT (*7*), a dopamine-insensitive protein that differs from BM3h-9D7 by only four residues and exhibits similar r_1 at 25°C (*8*). No significant signal changes were observed with BM3h-WT ($P = 0.25$, $n = 7$), indicating that the dopamine-binding property of BM3h-9D7 is necessary for MRI-detectable responses near the contrast agent injection site.

Fixed-potential amperometric recordings from separate animals ($n = 7$) treated identically to the MRI subjects confirmed that substantial dopamine release takes place in the area where MRI signal changes were recorded (Fig. 1, F and G); maximal concentrations of 17 ± 5 μM were detected. Electrochemical and MRI-based measurements showed similar temporal properties, with little adaptation of responses over multiple stimuli and similar onset kinetics after each stimulus. MRI recordings showed slower return to baseline, however. Amperometry after infusion of BM3h-9D7 ($n = 4$) showed stimulus-evoked dopamine release of only 0.59 ± 0.27 μM, significantly lower than measurements obtained in the absence of sensor (Student's *t* test, $P = 0.0092$) (Fig. 1H). By contrast, recordings after injection of BM3h-WT ($n = 3$) were indistinguishable from recordings without contrast agent ($P = 0.84$). BM3h-9D7 thus binds to stimulus-evoked dopamine in vivo, explaining the observed MRI contrast changes. Although dopamine buffering is a consequence of this interaction, buffering is unlikely to be severe near synapses, where dopamine transients probably exceed 1 mM (*11*).

Imaging data from the seven animals of Fig. 1E were coregistered, and a map of peak MRI changes was assembled (Fig. 2A). Signal changes were concentrated near the area of contrast agent injection. To distinguish regions that experienced little dopamine release from those that did not receive contrast agent, we used experimental parameters to model the expected MRI signal change as a function of sensor and dopamine concentration (Fig. 2B) (see materials and methods). The percentage of MRI signal change was a pseudolinear function of dopamine concentration up to a saturation point dependent on the voxel concentration of BM3h-9D7. By considering only those voxels (fig. S3) that experienced statistically significant ≥3.4% signal change during contrast agent injection, equivalent to ≥20 μM BM3h-9D7, we could obtain quantitative maps of released dopamine concentrations from individual fMRI data sets and averaged across animals.

We constructed a map of peristimulus dopamine concentration maxima across ventral striatum

and surrounding regions (Fig. 2C). Line profiles in Fig. 2C indicate error margins around the measured dopamine values and validate prominent features of the spatial map. Peak concentrations measured by molecular fMRI corresponded fairly closely to the electrochemical measurements of Fig. 1H. The most pronounced focus of MRI-detectable neurotransmitter release was found in the nucleus accumbens (NAc) core (NAcC), where dopamine concentrations reached 27 μM. Some areas that received substantial contrast agent doses showed little dopamine release.

Molecular fMRI allowed dynamic dopamine mapping over each MFB stimulus cycle (Fig. 3A). Average time courses for nine anatomically defined ROIs (Fig. 3B) were determined and fit to a simple model in which dopamine is released at a fixed rate during stimulation and removed according to a first-order rate constant. This model accounted well (squared correlation coefficent $R^2 \geq 0.9$) for data from eight regions (Fig. 3, C and D). Significant dopamine release rates (Student's t test, $P < 10^{-7}$) were found in all ROIs, though the quality of the fit to one region, the preoptic area (PO), was poor ($R^2 = 0.40$). The highest dopamine release rate (1.28 ± 0.04 μM/s) was observed in rostral NAcC (rNAcC), where peak dopamine amplitudes were highest (compare to Fig. 2C). Release rates in neighboring structures were ~30% lower, and differences in estimated release between rNAcC and all other ROIs were statistically significant (Student's t test, $P < 10^{-4}$). Apparent dopamine removal rates averaged 0.026 s^{-1}. Most pairwise differences among ROIs were insignificant ($P > 0.13$). Only ventral caudate putamen (vCPu) showed significantly higher removal than rostral and caudal NAc shell (rNAcS and cNAcS) and caudal NAcC (cNAcC). Dopamine removal and release rates were uncorrelated ($r = –0.39$, $P = 0.3$). Transport parameters were probably affected by binding kinetics of dopamine to BM3h-9D7 itself ($k_{obs} \sim 0.3$ s^{-1} for 20 μM sensor; fig. S4). Results nevertheless indicate that the profile of phasic dopamine amplitudes observed here can be explained by single compartment dynamics arising primarily from differences in stimulus-associated dopamine release, as opposed to dopamine elimination or catabolism.

We addressed the possibility that the electrode position in LH, which varied slightly in our experiments, influenced the spatial profile of dopamine responses measured by MRI. Response centroids were clustered within a sphere of ~1 mm diameter in NAc and showed no systematic relation to electrode positions (fig. S5A). This suggests that dopamine profiles do not purely reflect architecture of projections from the stimulation sites in LH (*12*). We also examined the relation between dopamine response amplitudes and stimulation coordinates (fig. S5B). Significant correlation between rostrocaudal electrode position and response magnitude was observed ($r = –0.97$, $P = 0.001$); mediolateral and dorsoventral electrode coordinates were uncorrelated ($P > 0.3$). Apparent dependence of dopamine release on rostrocaudal positioning of the stimulation site within a narrow spatial range (0.9 mm) suggests that ventral striatal dopamine release is modulated by distinct neural populations that were stimulated to varying extents.

Our molecular fMRI results offer insights related to dopaminergic signaling: First, among brain regions analyzed, rNAcC displayed maximal dopamine transients evoked by MFB stimulation. The observation of peak release in rNAcC is consistent with point measurements obtained with similar stimuli (*13*–*15*), but could not be predicted from immunohistological (*16*, *17*) or connectivity data (*18*). Second, the relation between stimulation coordinates and responses suggests that local circuitry near the stimulation site can modulate the amplitude of striatal dopamine release. The spatial profile of dopamine signaling did not vary strongly with stimulus location, but might relate to operant behavior. Third, the reward-related stimulation that we used promotes substantial phasic dopamine release outside NAc, where dopamine is less studied. Examination of an extended field of view even showed evidence of extrastriatal dopamine release in the thalamic reticular nucleus (fig. S6). Fourth, molecular fMRI data presented here provide an unprecedented microscopically averaged measure of phasic dopamine, including contributions from multiple extracellular environments. Approximate quantitative agreement between imaging and electrochemical measurements argues for functional equivalence of these techniques and corroborates validity of interstitial dopamine as a surrogate indicator of synaptic neurotransmitter release (*19*).

This work establishes a foundation for extension of molecular fMRI techniques along multiple trajectories. Relationships between dopamine signaling and other components of neural activity could be analyzed by combining our dopamine imaging method with conventional hemodynamic fMRI or additional molecular fMRI approaches. Higher-resolution imaging could be performed to characterize signaling at spatial scales below 100 μm. Sensitivity would be enhanced beyond concentrations of 2 to 5 μM dopamine achieved here by using better contrast agents or different imaging parameters, and improved probe delivery strategies could enable completely noninvasive experiments. These steps will facilitate application of molecular fMRI to numerous problems in neuroscience.

References and Notes

1. A. Jasanoff, *Curr. Opin. Neurobiol.* **17**, 593–600 (2007).
2. J. D. Salamone, M. Correa, *Neuron* **76**, 470–485 (2012).
3. W. Schultz, *Trends Neurosci.* **30**, 203–210 (2007).
4. D. Sulzer, *Neuron* **69**, 628–649 (2011).
5. S. Ikemoto, *Brain Res. Brain Res. Rev.* **56**, 27–78 (2007).
6. M. P. Saddoris, J. A. Sugam, F. Cacciapaglia, R. M. Carelli, *Front. Biosci.* **E5**, 273 (2013).
7. M. G. Shapiro *et al.*, *Nat. Biotechnol.* **28**, 264–270 (2010).
8. E. M. Brustad *et al.*, *J. Mol. Biol.* **422**, 245–262 (2012).
9. A. G. Ewing, J. C. Bigelow, R. M. Wightman, *Science* **221**, 169–171 (1983).
10. L. J. May, W. G. Kuhr, R. M. Wightman, *J. Neurochem.* **51**, 1060–1069 (1988).
11. P. A. Garris, E. L. Ciolkowski, P. Pastore, R. M. Wightman, *J. Neurosci.* **14**, 6084–6093 (1994).
12. R. Nieuwenhuys, L. M. Geeraedts, J. G. Veening, *J. Comp. Neurol.* **206**, 49–81 (1982).
13. S. R. Jones, S. J. O'Dell, J. F. Marshall, R. M. Wightman, *Synapse* **23**, 224–231 (1996).
14. N. A. Addy, D. P. Daberkow, J. N. Ford, P. A. Garris, R. M. Wightman, *J. Neurophysiol.* **104**, 922–931 (2010).
15. J. Park, B. J. Aragona, B. M. Kile, R. M. Carelli, R. M. Wightman, *Neuroscience* **169**, 132–142 (2010).
16. B. J. Ciliax *et al.*, *J. Neurosci.* **15**, 1714–1723 (1995).
17. C. Freed *et al.*, *J. Comp. Neurol.* **359**, 340–349 (1995).
18. D. S. Zahm, *Ann. N.Y. Acad. Sci.* **877**, 113–128 (1999).
19. S. J. Cragg, M. E. Rice, *Trends Neurosci.* **27**, 270–277 (2004).
20. G. Paxinos, C. Watson, *The Rat Brain in Stereotaxic Coordinates* (Academic Press, San Diego, CA, ed. 3, 1997).

Acknowledgments: This work was supported by NIH grants R01-DA02899, R01-NS076462 and DP2-OD002114, and Defense Advanced Research Projects Agency grant W911NF-10-0059 to A.J. We thank G. Westmeyer for technical guidance and A. Graybiel for comments on the manuscript. We also thank C. Blaha, A. Graybiel, M. Howe, T. Rogers, and T. Schneider for assistance with electrochemistry; E. Brustad and F. Arnold for collaboration on sensor development; and A. Liang and S. Lippard for help with stopped-flow measurements. U.S. patent application 12/675,256 pertains to BM3h-9D7.

Supplementary Materials

www.sciencemag.org/content/344/6183/533/suppl/DC1
Materials and Methods
Figs. S1 to S6
Reference (*21*)

5 December 2013; accepted 3 April 2014
10.1126/science.1249380

Science

Molecular-Level Functional Magnetic Resonance Imaging of Dopaminergic Signaling

Taekwan Lee, Lili X. Cai, Victor S. Lelyveld, Aviad Hai and Alan Jasanoff

Science **344** (6183), 533-535.
DOI: 10.1126/science.1249380

Watching Brain Molecules

Functional neuroimaging using magnetic resonance imaging (MRI) molecular sensors would be useful for mechanistic analysis of neural systems. **Lee *et al.*** (p. 533) applied MRI-detectable sensors to measure molecular aspects of brain function in conjunction with noninvasive imaging. The molecular sensor revealed a quantitative spatiotemporal map of dopamine release in the ventral striatum, a brain area involved in processing rewards.